Nanorheology with a Conventional Rheometer: Probing the Interfacial Properties in Compatibilized Multinanolayer Polymer Films

Quentin Beuguel,*[,†] Alain Guinault,[†] Liliane Léger,[‡] Frédéric Restagno,[‡] Cyrille Sollogoub,[†] and Guillaume Miquelard-Garnier*[,†]

[†]Laboratoire PIMM, Arts et Métiers, CNRS, CNAM, Hesam Université, 151 Boulevard de l'Hôpital, 75013 Paris, France
[‡]Laboratoire de Physique des Solides, CNRS, Univ Paris-SUD, Université Paris-Saclay, 91405 Orsay, Cedex, France

ABSTRACT: Measuring the viscoelastic behavior of polymers in the vicinity of a surface or under confinement is an experimental challenge. Simple rheological tests of nanolayered films of polyethylene/polyamide 6 compatibilized in situ during the coextrusion process enabled the probing of these interfacial properties. Taking advantage of the different melting points and of the multiplication of the number of interfaces, a drastic increase of dynamic moduli was reported when increasing the interphase volume fraction in the films. A solid-like behavior for the interphase was identified. The complex viscosity of nanolayered films as a function of angular frequency was quantitatively captured for all samples using a weighted mixing law of bulk and interphase viscosities, without additional adjusting parameters, highlighting the interfacial synergy developed in nanolayered polymer films.

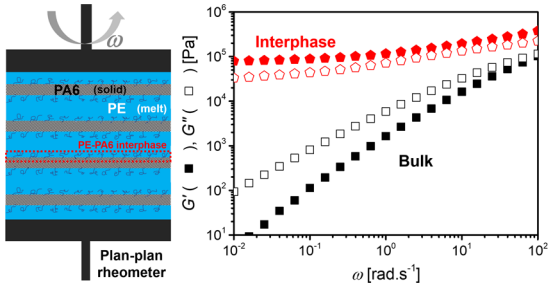

Simple or complex fluids can display very different rheological properties under nanometric confinement or in the vicinity of surfaces, compared to the bulk one.[1] Several nanorheological tools[2] have been developed to capture both static and dynamics of confined liquids, such as an atomic force microscope (AFM),[3] surface forces apparatus (SFA),[4] and motion tracking of fluorescent fluid[5] or nanoparticles.[6] These experiments have improved the fundamental comprehension of the rheological behavior of fluids in conditions where at least one dimension approaches the molecular size. However, they are fairly complicated and have sometimes led to seemingly contradictory results, possibly due to experimental artifacts. Examples of such controversies includes the determination of the hydrodynamic boundary condition of water on hydrophobic surfaces[7] or the role of free interfaces on the macromolecular mobility[8,9] and glass transition[10] in ultrathin polymer films.

Moreover, the consequences of the physical models derived from such "idealized" experiments have been only scarcely applied to industrial materials where the local properties of interfaces yet govern the macroscopic properties. For example, in immiscible polymer blends,[11] the role of interfacial adhesion is crucial.[12] At the interfaces, the interpenetration between the two immiscible polymers typically occurs over a distance smaller than the entanglement one ($\lesssim$5 nm),[13] leading to poor mechanical properties. A well-known method in the industry to increase such properties, called compatibilization, is the addition of a third polymer, usually a copolymer[14] or a grafted polymer with reactive function,[15] which preferentially segregates at the interface, thickening it and forming an "interphase" ($\gtrsim$10 nm).[16] The interphase rheological properties control adhesion between immiscible polymers,[17] but quantitative measurement of these properties is lacking in the literature.

Moan et al.[18] correlated the modification of the viscoelastic properties of immiscible blends by the addition of a compatibilizer with the appearance of an additional long relaxation time, attributed to the interphase. Zhao and Macosko[19] have used multilayer blend morphologies to amplify and model the role of the interphase in the rheological response. In noncompatibilized systems with 64 microlayers, a drop in viscosity at high shear rates was attributed to interfacial slip. This interfacial slip led to a decrease of interfacial adhesion,[20] suppressed in the presence of compatibilizer, preventing delamination of the multilayer.[21]

The aim of this study is to quantitatively measure the rheological properties of compatibilized interphases. We take advantage of a new coextrusion process enabling, via the use of layer multiplying elements (LME), the increase in the number of layers up to a few thousand, hence, a decrease in their thickness down to a few nanometers.[22,23] The associated huge increase in the interphase volume fraction further increases its

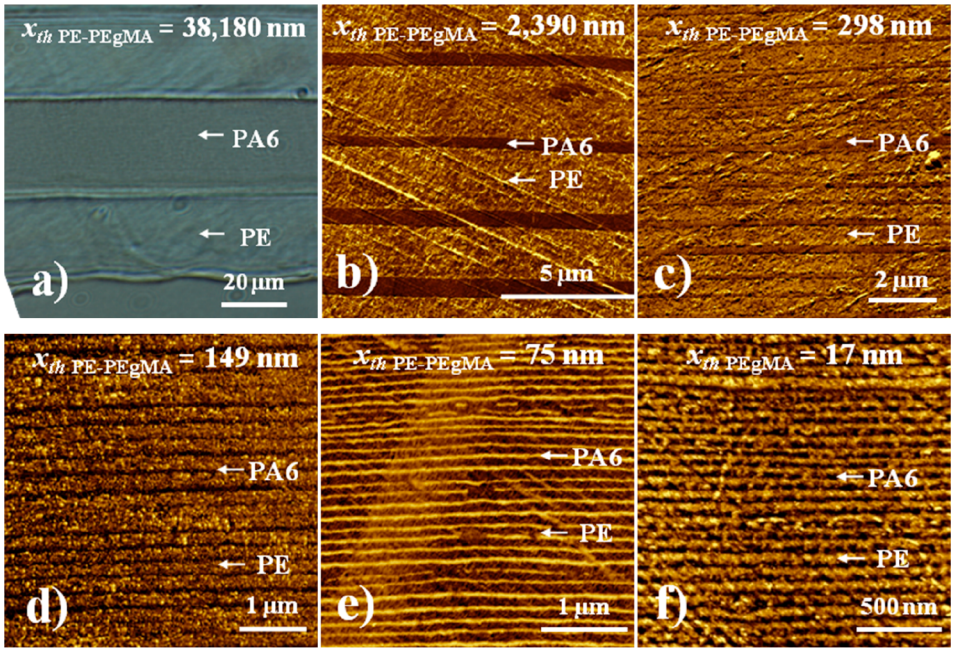

Figure 1. Optical (a) and AFM (b–f) images of PE/PEgMA/PA6 multilayer films

role in the macroscopic rheological response. We selected two semicrystalline immiscible polymers, polyethylene (PE) and polyamide 6 (PA6), generally associated in packaging films for their respective barrier and mechanical properties.[24] As described above, the addition of a compatibilizer as a tie layer, polyethylene-*graft*-maleic anhydride (PEgMA), forming a PE–PA6 copolymer in a few seconds[25] at the interface during coextrusion,[26] is required to improve the films' final properties.[27,28] These two polymers have different melting temperatures, which will allow the probing of the rheological response of the films with polymers in different states and amplify even more the interfacial related phenomena.

The multilayered morphology of PE/PEgMA/PA6 multilayer films is illustrated in Figure 1. The average experimental thicknesses of PE–PEgMA layers $x_{PE-PEgMA}$ and their standard deviation $std_{PE-PEgMA}$ were calculated from the measurement of at least 10% of the total number of layers.[29] They are reported in Table 1 and are in reasonable agreement with their respective theoretical thickness $x_{thPE-PEgMA}$. $std_{PE-PEgMA}$ appears slightly higher than for other multilayer systems,[29] which may be due to the relatively high viscosity ratios between polymers (Table S1, Supporting Information). Few layer breakups can be observed in Figure 1e only for the thinnest PA layer[23] and were considered negligible here.

Table 1. Dimensions of PE–PEgMA Layers in PE/PEgMA/PA6 Multilayer Films

fraction (wt %)	LME	x (μm)	$x_{thPE-PEgMA}$ (nm)	$x_{PE-PEgMA}$ (nm)	$std_{PE-PEgMA}$ (nm)
25/50/25	0	100	38180	31000	1600
	5		2390	2600	440
	8		298	400	120
	9		149	160	40
	8	25	75	75	30
0/33/67	9	25	17	20	5

During the extrusion, the maleic anhydride functions of PEgMA reacts with the amino-terminated PA6 to form PE–PA6 copolymers at the PE/PA6 interface.

For the PEgMA and PA6 molar masses of the study, the maximum surface density grafting is limited by PA6 due to its greater end-to-end distance and hence its larger macromolecular volume span (Table S1). The maximum surface density of PA6 chains in contact with the interface can be estimated as $\sigma = \frac{1}{N_{PA6}^{1/2} a_{PA6}^{2}} \sim 0.04$ chains·nm^{-2},[30] where a is the monomer length and N the degree of polymerization. At T = 180 °C, PA6 is in the solid state, while PE and PEgMA are in the molten state. Since PE has a higher degree of polymerization than PEgMA (Table S1), it is reasonable to consider the interphase in the PE layers as a PEgMA Gaussian brush grafted on a PA6 solid surface, interpenetrated by a miscible bulk of PE and PEgMA[31,32] down to the PA6 surface.[33] Its thickness is estimated as $x_i \sim a_{PEgMA} N_{PEgMA}^{1/2} \sim 15$ nm (Figure 2).[34]

The ratio between the available number of PEgMA chains in the multilayer films and the maximum surface density of PA6 chains at the interface can also be estimated as a function of the number of interfaces, taking into account the low grafting level of PEgMA chain (0.2 wt %, i.e., roughly one grafting unit per chain). It is found to vary between ~13300 to 7, for $x_{thPE-PEgMA}$ ranging from 38180 to 37 nm. As the processing time of coextrusion is long enough to achieve most of the compatibilization reaction,[35] we assume that the interphase is quasi-saturated and has a continuous identical thickness for all the films studied (Figure S1).

Figure 3 shows the evolution of elastic G' (a) and loss G'' (b) moduli as a function of angular frequency ω for PE–PEgMA bulk and PE/PEgMA/PA6 multilayer films, at T = 180 °C. The associated relaxation spectrum H(λ) is plotted in Figure 3c.[36] The complex viscosity η^* in the linear domain appears in Figure 3d.

First, let us note that under such oscillatory shear conditions, PA6 in the solid state does not contribute to the rheological

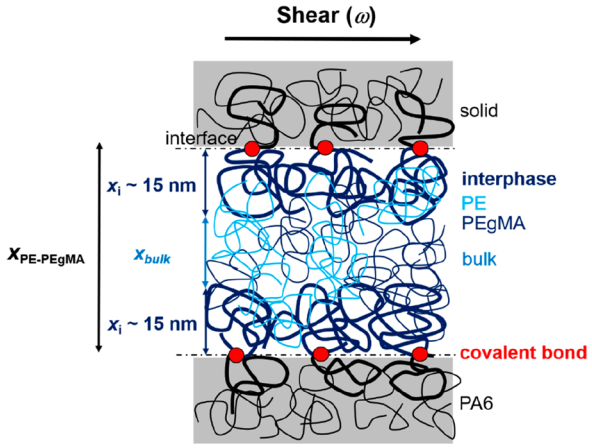

Figure 2. Schematic of three layers of compatibilized PE/PEgMA/PA6 film.

signal due to the multilayered structure. Hence, the viscoelastic properties will be governed by the PE−PEgMA phase.

From multimicrolayer film with $x_{th\mathrm{PE-PEgMA}}$ = 38180 nm and down to a nanolayer film with $x_{th\mathrm{PE-PEgMA}}$ = 37 nm, both elastic G' (Figure 3a) and loss G'' (Figure 3b) moduli drastically increase compared to those of the PE−PEgMA bulk, especially at low angular frequencies ω. At low frequencies, it is possible to define G'_0 and the G''_0 plateau moduli that progressively appear, corresponding to a solid-like behavior that is observed for the films with the thinnest layers. A very significant increase of ~4 and 3 decades on, respectively, G' and G'' is recorded at low angular frequencies ω, much higher than what is measured on multilayer systems with both phases in the molten state.[19] At high frequencies, the behavior of all systems approach that of the PE−PEgMA bulk matrix.

In Figure 3c, a relaxation time λ_m ~8×10^{-2} s is observed for all bulk and multilayer films. It is close to the melt reptation time of the bulk, $\lambda_{rept} = \frac{\zeta_{1PE} a_{PE}^2}{k_B T} \frac{N_{PE}}{N_{ePE}} \sim 1 \times 10^{-2}$ s,[37] where ζ_{1PE} is the monomeric friction parameter = 4.50×10^{-13} kg·s^{-1},[38] and N_{ePE} is the degree of polymerization between entanglements ~35.[39] This time is attributed to the terminal relaxation of bulk chains.[40,41] An additional long relaxation time λ_i ($\gtrsim$100 s) appears for all multilayer films, in agreement with Moan et al.[18] observations on compatibilized PE/PA12 blends. This long time λ_i could be related to the relaxation time of PE chains anchored to the PA6 solid surface (PE−PA6 copolymer) via the grafting reaction,[42] delaying the terminal relaxation of PE chains in the interphase formed.[43,44] Furthermore, λ_i and its peak intensity increases when PE−PEgMA layer thickness $x_{th\mathrm{PE-PEgMA}}$ decreases, hence, when the interphase volume fraction ϕ_i increases.

Figure 3d shows a conventional viscoelastic behavior of thermoplastic for PE−PEgMA bulk (black squares), exhibiting a Newtonian plateau at low angular frequencies ω. For the film with the thinnest PE−PEgMA layers (gray hollow hexagons), we assume that for such thickness ($x_{th\ \mathrm{PEgMA}}$ = 17 nm), similar to the estimated interphase one (x_i ~ 15 nm), we have pure interphase properties.[45] A rheo-thinning behavior is observed,

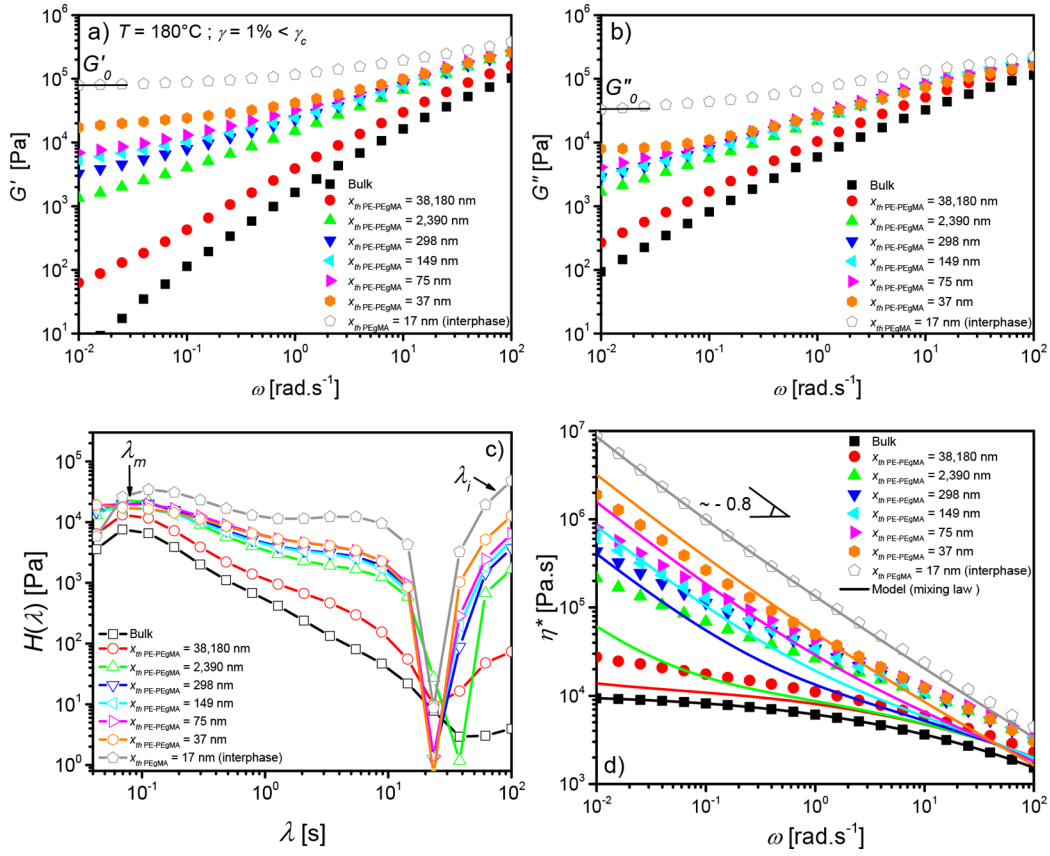

Figure 3. Elastic G' (a) and loss G'' (b) moduli and complex viscosity η^* (d) as a function of angular frequency ω, and associated relaxation spectrum $H(\lambda)$ (c) for PE/PEgMA/PA6 multilayer films. The lines (d) correspond to the multilayer film model using weighted mixing law for complex PE−PEgMA phase complex viscosity $\eta^*_{\mathrm{PE-PEgMA}}(\omega)$.

characterized by the universal power law of $\eta^* \sim \omega^{-0.8}$, assuming the empirical Cox–Merz relationship $\eta^*(\dot{\gamma}) = \eta^*(\omega)$,[46] suggested to be valid for all polymers.[47] The bulk and interphase viscosity $\eta^*_{bulk}(\omega)$ and $\eta^*_i(\omega)$ as a function of angular frequency can then be described using a phenomenological Carreau–Yasuda model,[48−51] including relaxation times λ_{bulk} and λ_i, without (for bulk (eq 1)) and with (for interphase (eq 2)) yield-stress, adapted to viscoelastic thermoplastics:

$$\eta^*_{bulk}(\omega) = \eta^*_{0bulk}[1 + (\lambda_{bulk}\omega)^{b_{bulk}}]^{n-1/b_{bulk}} \quad (1)$$

and

$$\eta^*_i(\omega) = \frac{\tau_{0i}}{\omega} + \eta^*_{0i}[1 + (\lambda_i\omega)^{b_i}]^{n-1/b_i} \quad (2)$$

with τ_{0i}, the apparent yield-stress, η^*_{0bulk} and η^*_{0i}, the Newtonian complex viscosities, b_{bulk} and b_i, fitting parameters, and n the pseudoplasticity index fixed to the same value for both phases = 0.2 (hence, $n - 1 = -0.8$).[47] For PE–PEgMA bulk, the extrapolated Newtonian complex viscosity at low angular frequencies ω gives $\eta^*_0 \sim 10630$ Pa·s and the relaxation time is $\lambda_{bulk} \sim 2 \times 10^{-2}$ s, similar to λ_m (Figure 3c) and λ_{rept}. Because of the shear thinning shape of the curve in the all angular frequency range ω for the system with only interphase in the PE–PEgMA phase ($x_{thPEgMA}$ = 17 nm), we fix, based on Figure 3c, but somewhat arbitrarily, λ_i = 100 s in the Carreau–Yasuda model in order to limit the number of possible couples of values (τ_{0i}, η^*_{0i}). It leads to $\tau_{0i} = 2.8 \times 10^4$ Pa and $\eta^*_{0i} = 2.1 \times 10^6$ Pa·s. The fitting parameters are b_{bulk} = 0.34 and b_i = 0.23. Let us note that a Carreau–Yasuda model without apparent yield stress (with a Newtonian plateau) and a relaxation time higher than 100 s or a simple power law model with a slope of −0.8 could also be used for interphase viscosity modeling.

All multilayer systems exhibit a yield behavior (Figure 3d), in agreement with results reported by Lamnawar et al.,[52] in the case of similar compatibilized bilayer films, and attributed to the presence of a PE–PA6 copolymers interphase. The yield is more pronounced for thin PE–PEgMA layers.

The complex viscosity η^* of immiscible multilayer films is generally described by a serial model (eq 3) considering no interaction between phases:[19,52−54]

$$\frac{1}{\eta^*(\omega)} = \frac{\phi_{PE-PEgMA}}{\eta^*_{PE-PEgMA}(\omega)} + \frac{\phi_{PA6}}{\eta^*_{PA6}(\omega)} \quad (3)$$

where $\phi_{PE-PEgMA}$ and ϕ_{PA6} are the volume fractions of PE and PA6 phases and $\eta^*(\omega)$, $\eta^*_{PE-PEgMA}(\omega)$, and $\eta^*_{PA6}(\omega)$ correspond to the apparent complex viscosity of the multilayer film, PE–PEgMA and PA6 layers (or phases), respectively. Because $\eta^*_{PA6} \gg \eta^*_{PE-PEgMA}$, the second term of (3) can be neglected. Using this relation, the interphase viscosity can be simply determined from the $\eta^*(\omega)$ values of the film $x_{thPEgMA}$ = 17 nm ($\eta^*_i(\omega) = 0.75\eta^*_{17nm\_multilayer\_film}(\omega)$). At high frequencies this interphase viscosity then roughly joins this of the bulk, in agreement with the Cohen et al.[55] measurement of the effective viscosity of sheared polydimethylsiloxane (PDMS) brushes with different molecular weights.

However, this relation does not adjust the rheological behavior of such multilayer films in the presence of an interphase, and many authors suggest the introduction of a third phase (in serial) for noncompatibilized[54] or compatibilized systems,[52] or interfacial slip velocity.[19] However, there is no interfacial slip evidence in the compatibilized system, according to Zhao and Macosko.[19] This is in agreement with the high critical shear rate calculated value for our PE/PEgMA/PA6 systems, $\dot{\gamma}^* = \frac{k_B T}{a_{PE} N_{ePE}^{1/2} a_{PA6}^2 N_{PA6}^{1/2} \eta^*_0} \sim 17\ s^{-1}$ at T = 180 °C, separating the domain between stretching (low slip) and disentanglement (high slip) of interpenetrated melt in anchored brush polymer chains on a solid surface.[56] In such a case, the noninteraction assumption in the serial model for a multilayered film is not valid, and the addition of an independent interphase viscosity is not possible. Thus, the viscosity profile of the PE–PEgMA layer is complex, and in order to consider the interactions between interphase and bulk, we use as a first approximation a simple weighted mixing law (eq 4):

$$\eta^*_{PE-PEgMA}(\omega) = \phi_{bulk}\eta^*_{bulk}(\omega) + \phi_i\eta^*_i(\omega) \quad (4)$$

where ϕ_{bulk}, ϕ_i, $\eta^*_{bulk}(\omega)$, and $\eta^*_i(\omega)$ represent the relative volume fraction of bulk and interphase in the PE–PEgMA layer and their associated viscosity (using eqs 1 and 2), respectively. In multilayer films, the volume fraction ϕ is directly related to the number of layers and their thickness (eq 5):

$$\phi_{PE-PEgMA} = \frac{\phi_{bulk} + \phi_i}{\phi_{bulk} + \phi_i + \phi_{PA6}} = \frac{n_{bulk}x_{bulk} + n_i x_i}{n_{bulk}x_{bulk} + n_i x_i + n_{PA6}x_{PA6}} \quad (5)$$

where n_{bulk}, n_i, n_{PA6}, x_{bulk}, x_i, and x_{PA6} correspond to the layer number and their associated thickness of PE–PEgMA bulk, interphase (in PE–PEgMA) and PA6, respectively. More precisely, for each system, x_i has been chosen to be equal to 15 nm, and the theoretical thicknesses (Table 1) have been attributed to x_{bulk} ($x_{bulk} = x_{thPE-PEgMA} - 2x_i$) and x_{PA6}.

This simple model enables to quantitatively predict the rheological behavior of compatibilized nanolayered PE/PEgMA/PA6 films without additional adjusting parameters (Figure 3d). Note that the general trend is relatively insensitive to the precise value attributed to x_i or the choice of experimentally measured thicknesses versus theoretical ones (Figure S2). As even the weighted mixing law systematically underestimates the experimental data, it reveals a synergistic effect between the interphase and the surrounding melt polymer, even for low interphase fractions. It highlights the crucial role of interphase volume fraction ϕ_i and confirms the interaction between bulk and interphase in compatibilized system, controlling adhesion properties.

In summary, the rheology of the interfacial layer has been quantitatively measured and is several orders of magnitude higher than the bulk one, similar to a network structure behavior. A synergistic effect between the grafted chains that constitutes the interphase and the melt polymer chains has been captured using a simple weighted mixing law. As future work, the complex viscosity profile of PE–PEgMA phase in such compatibilized systems will be investigated.

The multilayered coextrusion process coupled with simple macroscopic rheological tests, turning off one solid phase under shear, opens the way to quantitively characterize the rheological properties of interphases in immiscible polymer systems, whether compatibilized or not. This will help in a better understanding the role of this interphase in the final material properties.

EXPERIMENTAL SECTION

Sample Preparation. Three polymers were used in multilayer films: a linear low density polyethylene (PE, Dowlex 2645), a linear low density polyethylene-*graft*-maleic anhydride (PEgMA, Amplify TY1353) with a grafted level of 0.2 wt % (compatibilizer), both from Dow Chemical Company (Midland, U.S.A.), and a polyamide 6 (PA6, Ultramid B40), from BASF (Ludwigshafen, Germany). The main characteristics of these three polymers are reported in Table S1.

Multilayer films were elaborated using the coextrusion line previously described.[57,58] Briefly, three single-screw extruders were fed with PE, PEgMA, and PA6, and the polymer flows were then combined in a feed-block to build a five-layer film (PE (external layers), PEgMA (tie layers), and PA6 (internal layer)) at T = 240 °C, with a fixed composition (25/50/25 wt %). Then, the film passed successively through N = 0, 5, 8, or 9 LME, increasing the layer number n from 5 to 2049 ($n = 2^{N+2} + 1$) The films were cooled down on chill rolls regulated at T = 80 °C and stretched to two different final thicknesses, $x \sim 100$ and 25 μm, for every experimental condition. The theoretical nominal layer thickness of miscible PE−PEgMA layers was calculated from flow rate measurements, and ranged from $x_{th\mathrm{PE-PEgMA}}$ = 38180 to 37 nm for the different systems. A 0/33/67 wt % 9 LME 25 μm film with $x_{th\mathrm{PEgMA}}$ = 17 nm was also fabricated.

Morphological Characterization. Film morphology was observed along the transversal axis, using optical and atomic force microscopes (AFM; Supporting Information).[29]

Rheological Characterization. Before manipulation, the samples were dried under vacuum at 60 °C for 48 h. Then they were stacked and slightly compressed (~1 × 10^3 Pa) under vacuum at 140 °C for 30 min, which aimed at getting rid of air bubbles during the experiment, improving adhesion between stacked films and enabling PE and PEgMA chains relaxation. Controlled stress rheometer MCR 502 (Anton Paar, Austria), equipped with a plate/plate geometry was used in order to perform the linear viscoelastic tests, at T = 180 °C under nitrogen flow. A total of 16 (for x = 100 μm) or 32 (for x = 25 μm) multilayer films were stacked for manipulation convenience. Thus, the gap was set to ~1.6 or 0.8 mm depending on sample thickness. It was verified that there is no influence of the stacked film number on the rheological properties. At these temperatures, only the PE−PEgMA phase was in the molten state, while PA6 is in the solid state, similar to the work by Walczak[59] on polystyrene/polycarbonate multilayer films. In this condition, no significant additional amount of copolymer is formed at the interface during the experiment (Figure S1), and in consequence, the interphase properties were investigated as prepared.[30,60] The rheological properties of multilayer films were compared to those of PE−PEgMA bulk (33/67 wt %) under the same form of stacked films (T = 140 °C for 30 min) obtained from compressed blended pellets. Frequency sweep tests, with angular frequency ω ranging from 10^2 to 10^{-2} rad·s^{-1}, in the linear domain (at strain γ_0 = 0.01) were performed. The relaxation spectra $H(\lambda)$ were plotted using RSI Orchestrator software, based on G' and G'' frequency measurements.[36] The nanolayered structure of the films was confirmed using AFM after frequency sweep tests ($t \sim 90$ min), and the thermal stability in the linear domain (γ = 0.01 and ω = 0.1 rad·s^{-1}) of the systems was verified for t = 2 h at T = 180 °C. Based on duplicate measurements, the accuracy of rheological data was estimated to ±5%.

AUTHOR INFORMATION

Corresponding Authors

*E-mail: quentin.beuguel@lecnam.net.
*E-mail: guillaume.miquelardgarnier@lecnam.net.

ORCID

Frédéric Restagno: 0000-0001-7803-6677
Cyrille Sollogoub: 0000-0003-2204-3696
Guillaume Miquelard-Garnier: 0000-0002-0251-8941

Notes

The authors declare no competing financial interest.

ACKNOWLEDGMENTS

The authors thank the French National Research Agency (ANR) for its financial support (Project No. 16-CE08-0035, Coordinator S. Marais). We are grateful to F. Chinesta for fruitful discussions and to I. Iliopoulos for his relevant comments. The authors acknowledge E. Richaud and N. Longerias from PeakExpert (Tours, France) for gel permeation chromatography (GPC) analysis of PE/PEgMA and PA6, respectively. The authors would like to thank A. Grandmontagne for her help in coextrusion. We gratefully acknowledge S. Norvez and M. Cloitre, from the Ecole Supérieure de Physique et de Chimie Industrielle (ESPCI, Paris, France), for providing access to the ultracryomicrotome facility.

REFERENCES

(1) Lee, D. W.; Ruths, M.; Israelachvili, J. N. Surface Forces and Nanorheology of Molecularly Thin Films. *Nanotribology and Nanomechanics*; Springer International Publishing: Cham, 2017; pp 457−518, DOI: 10.1007/978-3-319-51433-8_9.

(2) Bocquet, L.; Charlaix, E. Nanofluidics, from Bulk to Interfaces. *Chem. Soc. Rev.* **2010**, *39* (3), 1073−1095.

(3) Nakajima, K.; Yamaguchi, H.; Lee, J.-C.; Kageshima, M.; Ikehara, T.; Nishi, T. Nanorheology of Polymer Blends Investigated by Atomic Force Microscopy. *Jpn. J. Appl. Phys.* **1997**, *36* (Part 1, No. 6B), 3850−3854.

(4) Restagno, F.; Crassous, J.; Charlaix, É.; Cottin-Bizonne, C.; Monchanin, M. A New Surface Forces Apparatus for Nanorheology. *Rev. Sci. Instrum.* **2002**, *73* (6), 2292−2297.

(5) Migler, K. B.; Hervet, H.; Leger, L. Slip Transition of a Polymer Melt under Shear Stress. *Phys. Rev. Lett.* **1993**, *70* (3), 287−290.

(6) Squires, T. M.; Mason, T. G. Fluid Mechanics of Microrheology. *Annu. Rev. Fluid Mech.* **2010**, *42* (1), 413−438.

(7) Cottin-Bizonne, C.; Cross, B.; Steinberger, A.; Charlaix, E. Boundary Slip on Smooth Hydrophobic Surfaces: Intrinsic Effects and Possible Artifacts. *Phys. Rev. Lett.* **2005**, *94* (5), 056102.

(8) Alcoutlabi, M.; McKenna, G. B. Effects of Confinement on Material Behaviour at the Nanometre Size Scale. *J. Phys.: Condens. Matter* **2005**, *17* (15), 461−524.

(9) Russell, T. P.; Chai, Y. 50th Anniversary Perspective : Putting the Squeeze on Polymers: A Perspective on Polymer Thin Films and Interfaces. *Macromolecules* **2017**, *50* (12), 4597−4609.

(10) Bäumchen, O.; McGraw, J. D.; Forrest, J. A.; Dalnoki-Veress, K. Reduced Glass Transition Temperatures in Thin Polymer Films: Surface Effect or Artifact? *Phys. Rev. Lett.* **2012**, *109* (5), 055701.

(11) Utracki, L. A.; Wilkie, C. A. In *Polymer Blends Handbook*; Utracki, L. A., Wilkie, C., Eds.; Springer Netherlands: Dordrecht, NL, 2014.

(12) Brown, H. R. The Adhesion of Polymers: Relations Between Properties of Polymer Chains and Interface Toughness. *J. Adhes.* **2006**, *82* (10), 1013−1032.

(13) Helfand, E.; Tagami, Y. Theory of the Interface between Immiscible Polymers. II. *J. Chem. Phys.* **1972**, *56* (7), 3592−3601.

(14) Creton, C.; Kramer, E. J.; Hadziioannou, G. Critical Molecular Weight for Block Copolymer Reinforcement of Interfaces in a Two-Phase Polymer Blend. *Macromolecules* **1991**, *24* (8), 1846−1853.
(15) Xanthos, M.; Dagli, S. S. Compatibilization of Polymer Blends by Reactive Processing. *Polym. Eng. Sci.* **1991**, *31* (13), 929−935.
(16) Li, H.; Chiba, T.; Higashida, N.; Yang, Y.; Inoue, T. Polymer−Polymer Interface in Polypropylene/Polyamide Blends by Reactive Processing. *Polymer* **1997**, *38* (15), 3921−3925.
(17) Léger, L.; Raphaël, E.; Hervet, H. Surface-Anchored Polymer Chains: Their Role in Adhesion and Friction. In *Polymer in Confined Environments*; Granick, S., Binder, K., Gennes, P.-G., Giannelis, E. P., Grest, G. S., Hervet, H., Krishnamoorti, R., Léger, L., Manias, E., Raphaël, E., Wang, S. Q., Eds.; Advances in Polymer Science; Springer: Berlin, Heidelberg, DE, 1999; Vol. *138*, pp 185−225, DOI: 10.1007/3-540-69711-X_5.
(18) Moan, M.; Huitric, J.; Médéric, P.; Jarrin, J. Rheological Properties and Reactive Compatibilization of Immiscible Polymer Blends. *J. Rheol.* **2000**, *44* (6), 1227−1245.
(19) Zhao, R.; Macosko, C. W. Slip at Polymer−Polymer Interfaces: Rheological Measurements on Coextruded Multilayers. *J. Rheol.* **2002**, *46* (1), 145−167.
(20) Zhang, J.; Lodge, T. P.; Macosko, C. W. Interfacial Slip Reduces Polymer-Polymer Adhesion during Coextrusion. *J. Rheol.* **2006**, *50* (1), 41−57.
(21) Khariwala, D.; Ling, M.; Hiltner, A.; Baer, E. Effect of the Tie-Layer Thickness on the Delamination and Tensile Properties of Polypropylene/Tie-Layer/Nylon 6 Multilayers. *J. Appl. Polym. Sci.* **2011**, *121* (4), 1999−2012.
(22) Ponting, M.; Hiltner, A.; Baer, E. Polymer Nanostructures by Forced Assembly: Process, Structure, and Properties. *Macromol. Symp.* **2010**, *294* (1), 19−32.
(23) Bironeau, A.; Salez, T.; Miquelard-Garnier, G.; Sollogoub, C. Existence of a Critical Layer Thickness in PS/PMMA Nanolayered Films. *Macromolecules* **2017**, *50* (10), 4064−4073.
(24) Wagner, J. R., Jr In *Multilayer Flexible Packaging*, 2nd ed.; Andrew, W., Ed.; ElsevierOxford, UK, 2016.
(25) Orr, C.; Cernohous, J. J.; Guegan, P.; Hirao, A.; Jeon, H. K.; Macosko, C. W. Homogeneous Reactive Coupling of Terminally Functional Polymers. *Polymer* **2001**, *42* (19), 8171−8178.
(26) Lechner, F. The Co-Rotating Twin-Screw Extruder for Reactive Extrusion. *Reactive Extrusion*; Wiley-VCH Verlag GmbH & Co. KGaA: Weinheim, Germany, 2017; pp 11−35, DOI: 10.1002/9783527801541.ch2.
(27) Du, Q.; Jiang, G.; Li, J.; Guo, S. Adhesion and Delamination Failure Mechanisms in Alternating Layered Polyamide and Polyethylene with Compatibilizer. *Polym. Eng. Sci.* **2010**, *50* (6), 1111−1121.
(28) Jiang, G.; Zhang, F.; Wu, H.; Yan, B.; Guo, S. Comparative Studies on Enhanced Interfacial Adhesion between PE and PA6 through Two Routes in a Sequential Injection Molding Process. *Polym.-Plast. Technol. Eng.* **2014**, *53* (1), 9−18.
(29) Bironeau, A.; Dirrenberger, J.; Sollogoub, C.; Miquelard-Garnier, G.; Roland, S. Evaluation of Morphological Representative Sample Sizes for Nanolayered Polymer Blends. *J. Microsc.* **2016**, *264* (1), 48−58.
(30) Barraud, T.; Restagno, F.; Devisme, S.; Creton, C.; Léger, L. Formation of Diblock Copolymers at PP/PA6 Interfaces and Their Role in Local Crystalline Organization under Fast Heating and Cooling Conditions. *Polymer* **2012**, *53* (22), 5138−5145.
(31) Aubouy, M.; Raphaël, E. Structure of an Irreversibly Adsorbed Polymer Layer Immersed In. *Macromolecules* **1994**, *27* (18), 5182−5186.
(32) Aubouy, M.; Fredrickson, G. H.; Pincus, P.; Raphaël, E. End-Tethered Chains in Polymeric Matrixes. *Macromolecules* **1995**, *28* (8), 2979−2981.
(33) Marzolin, C.; Auroy, P.; Deruelle, M.; Folkers, J. P.; Léger, L.; Menelle, A. Neutron Reflectometry Study of the Segment-Density Profiles in End-Grafted and Irreversibly Adsorbed Layers of Polymer in Good Solvents. *Macromolecules* **2001**, *34* (25), 8694−8700.
(34) A refined calculation assumes the following: (i) shorter PEgMA chains are more likely to migrate towards the interface; (ii) maleic anhydride groups are randomly distributed on PEgMA chains, and some chains will have more than one graft; (iii) the stiffness of the polymer through the Flory's characteristic ratio C_∞. This leads to $x_i \approx a_{\mathrm{PEgMA}}\left(C_\infty \frac{M_{n\_\mathrm{PEgMA}}}{2 \times M_{0\mathrm{PE}}}\right)^{1/2} \approx 14$ nm.
(35) Kiparissoff-Bondil, H.; Devisme, S.; Rauline, D.; Chopinez, F.; Restagno, F.; Léger, L. Evidences for Flow-Assisted Interfacial Reaction in Coextruded PA6/PP/PA6 Films. *Polym. Eng. Sci.* **2019**, *59*, E44−E50.
(36) Honerkamp, J.; Weese, J. A Nonlinear Regularization Method for the Calculation of Relaxation Spectra. *Rheol. Acta* **1993**, *32* (1), 65−73.
(37) de Gennes, P. G. Reptation of a Polymer Chain in the Presence of Fixed Obstacles. *J. Chem. Phys.* **1971**, *55* (2), 572−579.
(38) Padding, J. T.; Briels, W. J. Zero-Shear Stress Relaxation and Long Time Dynamics of a Linear Polyethylene Melt: A Test of Rouse Theory. *J. Chem. Phys.* **2001**, *114* (19), 8685−8693.
(39) Szántó, L.; Vogt, R.; Meier, J.; Auhl, D.; Van Ruymbeke, E.; Friedrich, C. Entanglement Relaxation Time of Polyethylene Melts from High-Frequency Rheometry in the Mega-Hertz Range. *J. Rheol.* **2017**, *61* (5), 1023−1033.
(40) Rouse, P. E. A. Theory of the Linear Viscoelastic Properties of Dilute Solutions of Coiling Polymers. *J. Chem. Phys.* **1953**, *21* (7), 1272−1280.
(41) Doi, M.; Edwards, S. F. *The Theory of Polymer Dynamics*; Oxford University Press, Inc.: New York, USA, 1988.
(42) Brochard-Wyart, F.; Ajdari, A.; Leibler, L.; Rubinstein, M.; Viovy, J. L. Dynamics of Stars and Linear Chains Dissolved in a Polymer Melt. *Macromolecules* **1994**, *27* (3), 803−808.
(43) Vignaux-Nassiet, V.; Allal, A.; Montfort, J. P. Emulsion Models and Rheology of Filled Polymers. *Eur. Polym. J.* **1998**, *34* (3−4), 309−322.
(44) Chennevière, A.; Drockenmuller, E.; Damiron, D.; Cousin, F.; Boué, F.; Restagno, F.; Léger, L. Quantitative Analysis of Interdigitation Kinetics between a Polymer Melt and a Polymer Brush. *Macromolecules* **2013**, *46* (17), 6955−6962.
(45) Liu, R. Y. F.; Bernal-Lara, T. E.; Hiltner, A.; Baer, E. Interphase Materials by Forced Assembly of Glassy Polymers. *Macromolecules* **2004**, *37* (18), 6972−6979.
(46) Cox, W. P.; Merz, E. H. Correlation of Dynamic and Steady Flow Viscosities. *J. Polym. Sci.* **1958**, *28* (118), 619−622.
(47) Graessley, W. W. *The Entanglement Concept in Polymer Rheology; Advances in Polymer Science*; Springer-Verlag: Berlin/Heidelberg, 1974; Vol. *16*, DOI: 10.1007/BFb0031036.
(48) Byron Bird, R.; Carreau, P. J. A Nonlinear Viscoelastic Model for Polymer Solutions and Melts—I. *Chem. Eng. Sci.* **1968**, *23* (5), 427−434.
(49) Carreau, P. J.; MacDonald, I. F.; Bird, R. B. A Nonlinear Viscoelastic Model for Polymer Solutions and Melts—II. *Chem. Eng. Sci.* **1968**, *23* (8), 901−911.
(50) Yasuda, K.; Armstrong, R. C.; Cohen, R. E. Shear Flow Properties of Concentrated Solutions of Linear and Star Branched Polystyrenes. *Rheol. Acta* **1981**, *20* (2), 163−178.
(51) Macosko, C. W. *Rheology: Principles, Measurements and Applications*; Wiley-VCH: New York, U.S.A., 1994, DOI: 10.1016/S0032-5910(96)90008-X.
(52) Lamnawar, K.; Maazouz, A. Rheology and Morphology of Multilayer Reactive Polymers: Effect of Interfacial Area in Interdiffusion/Reaction Phenomena. *Rheol. Acta* **2008**, *47* (4), 383−397.
(53) Lin, C.-C. A Mathematical Model for Viscosity in Capillary Extrusion of Two-Component Polyblends. *Polym. J.* **1979**, *11* (3), 185−192.
(54) Carriere, C. J.; Ramanathan, R. Multilayer Rheology: A Comparison of Experimental Data with Modeling of Multilayer Shear Flow. *Polym. Eng. Sci.* **1995**, *35* (24), 1979−1984.

(55) Cohen, C.; Restagno, F.; Poulard, C.; Léger, L. Incidence of the Molecular Organization on Friction at Soft Polymer Interfaces. *Soft Matter* **2011**, *7* (18), 8535−8541.
(56) Brochard-Wyart, F.; Gay, C.; de Gennes, P.-G. Slippage of Polymer Melts on Grafted Surfaces. *Macromolecules* **1996**, *29* (1), 377−382.
(57) Nassar, S. F.; Domenek, S.; Guinault, A.; Stoclet, G.; Delpouve, N.; Sollogoub, C. Structural and Dynamic Heterogeneity in the Amorphous Phase of Poly(L,L -Lactide) Confined at the Nanoscale by the Coextrusion Process. *Macromolecules* **2018**, *51* (1), 128−136.
(58) Montana, J.-S.; Roland, S.; Richaud, E.; Miquelard-Garnier, G. From Equilibrium Lamellae to Out-of-Equilibrium Cylinders in Triblock Copolymer Nanolayers Obtained via Multilayer Coextrusion. *Polymer* **2018**, *136*, 27−36.
(59) Walczak, M. Properties of the Confined Amorphous Phase of Polymers. *Ph.D. Thesis*, Ecole Nationale Supérieure des Arts et Métiers, Paris (France), 2012.
(60) Bidaux, J.; Smith, G. D.; Bernet, N.; Månson, J.-A. E.; Hilborn, J. Fusion Bonding of Maleic Anhydride Grafted Polypropylene to Polyamide 6 via in Situ Block Copolymer Formation at the Interface. *Polymer* **1996**, *37* (7), 1129−1136.